 doi:10.20944/preprints202208.0010.v1

Article

Deep Deconvolution of Object Information Modulated by a Refractive Lens Using Lucy-Richardson-Rosen Algorithm

P. A. Praveen[1], Francis Gracy Arockiaraj[2], Shivasubramanian Gopinath[3], Daniel Smith[4], Tauno Kahro[1], Sandhra-Mirella Valdma[1], Andrei Bleahu[1], Soon Hock Ng[4], Andra Naresh Kumar Reddy[5,6], Tomas Katkus[4], Aravind Simon John Francis Rajeswary[1], Rashid. A Ganeev[5,7], Siim Pikker[1], Kaupo Kukli[1], Aile Tamm[1], Saulius Juodkazis[4,8], and Vijayakumar Anand[1,4]

[1] Institute of Physics, University of Tartu, W. Ostwaldi 1, 50411 Tartu, Estonia; praveen@ut.ee; tauno.kahro@ut.ee; sandhra-mirella.valdma@ut.ee; andreibleahu@gmail.com; aravind.simon.john.francis.rajeswari@ut.ee; siim.pikker@ut.ee; kaupo.kukli@ut.ee; aile.tamm@ut.ee; vijayakumar.anand@ut.ee
[2] PG & Research Department of Physics, The American College, Madurai 625009, India; francis-gracy646@gmail.com
[3] PG & Research Department of Physics, Thiagarajar College, Madurai 625009, India; gopishiva62@gmail.com
[4] Optical Sciences Center, Swinburne University of Technology, Melbourne 3122, Australia; danielsmith@swin.edu.au; soonhockng@swin.edu.au; tkatkus@swin.edu.au; sjuodkazis@swin.edu.au; vanand@swin.edu.au
[5] Laboratory of nonlinear optics, University of Latvia, Riga, LV – 1004, Latvia; naarereddy@gmail.com; rashid.ganeev@lu.lv
[6] Hee Photonic Labs, Riga, LV – 1002, Latvia;
[7] Tashkent Institute of Irrigation and Agricultural Mechanization Engineers, National Research University, Tashkent 100000, Uzbekistan;
[8] Tokyo Tech World Research Hub Initiative (WRHI), School of Materials and Chemical Technology, Tokyo Institute of Technology, 2-12-1, Ookayama, Meguro-ku, Tokyo 152-8550, Japan;
* Correspondence: vijayakumar.anand@ut.ee; praveen@ut.ee

Abstract: A refractive lens is one of the simplest, cost-effective and easily available imaging elements. With a spatially incoherent illumination, a refractive lens can faithfully map every object point to an image point in the sensor plane, when the object and image distances satisfy the imaging conditions. However, static imaging is limited to the depth of focus, beyond which the point-to-point mapping can be only obtained by changing either the location of the lens or the imaging sensor. In this study, the depth of focus of a refractive lens in static mode has been expanded using a recently developed computational reconstruction method, Lucy-Richardson-Rosen algorithm (LRRA). The technique consists of three steps. In this first step, the point spread functions (PSFs) were recorded along different depths and stored in the computer as PSF library. In the next step, the object intensity distribution was recorded. The LRRA was then applied to deconvolve the object information from the recorded intensity distributions in the final step. The results of LRRA were compared against two well-known reconstruction methods namely Lucy-Richardson algorithm and non-linear reconstruction.

Keywords: imaging; incoherent optics; Lucy-Richardson-Rosen algorithm; deblurring; refractive lens; computational imaging; holography; 3D imaging; deconvolution.

1. Introduction

Imaging objects using spatially incoherent light sources have many advantages such as higher imaging resolution and lower imaging noises such as edge ringing or speckle noises in comparison to coherent sources [1]. Furthermore, the use of spatially incoherent light sources is economical and eye safe. So, the development of incoherent imaging technologies is essential to utilize their advantages for imaging applications and as a matter of fact, in many cases such as astronomical imaging and fluorescence microscopy, they are irreplaceable [2]. While realizing a 2D incoherent imaging system is easy with a single

 doi:10.20944/preprints202208.0010.v1

refractive lens, extending the imaging dimensionality to 3D is a challenging task without introducing dynamic changes to the system. Three-dimensional imaging using spatially incoherent sources followed two directions of development. The first direction is based on the principles of holography involving two beam interferences, phase-shifting, generation of a complex hologram and image reconstruction by numerical back propagation [3-6]. This direction required extremely complicated optical architectures with numerous optical components due to the constraints of low coherence lengths. Some notable architectures developed in this direction are the rotational shearing interferometer [7], conoscopic holography [8], Fresnel incoherent correlation holography (FINCH) [9,10], Fourier incoherent single channel holography [11] and coded aperture correlation holography [12]. FINCH, which is considered as one of the simplest incoherent digital holography architectures requires an active device such as a spatial light modulator and multiple optical and opto-mechanical components.

An alternative research direction of 3D imaging using incoherent light was based on deconvolution, utilizing the linearity conditions of incoherent imaging. This approach, unlike the holography method, does not require two beam interferences, vibration isolation and many optical components. The first report of deconvolution-based imaging was reported by Dicke and Ables [13, 14]. In these studies, a random pinhole array was used as the only optical element between the object and the sensor. The scattered intensity distribution for an object was recorded, which was deconvolved into the object information using the pre-recorded point spread function (PSF). In comparison to the holography-based 3D imaging approaches, the deconvolution-based approach is faster, simpler, economical and compact.

The above research directions are not free of challenges and involved many decades of evolution until the ideas met the technology and vice versa [1,4,15,16]. The incoherent holography methods waited for the development of active optical devices such as SLM and the idea of FINCH. The deconvolution-based methods waited for the development of high-performance computational algorithms and the idea to image in 3D. The deconvolution based 2D imaging was reported in 1968, while the first 3D spatial imaging was reported in 2017 [17]. Most of the deconvolution -based 3D [18-20], 4D [21] and 5D [22,23] imaging techniques were reported in the last five years. In of all the above studies, a diffuser type optical modulator was used between the object and the sensor. Consequently, the signal to noise ratio (SNR) was low in all the above studies. The choice of the optical modulator originated from the requirements of the computational reconstruction algorithm. As most, if not all computational algorithms are correlation based, the autocorrelation function is required to be as sharp as possible to sample the object function [24,25]. The scattered intensity distributions in the far-field generate a sharp autocorrelation function as the average speckle size is equal to the diffraction limited spot size allowing diffraction limited imaging.

As diffusers are lossy and affect the SNR, it is necessary to find optical fields that can concentrate light in a small area on the sensor. A recent review from our research group identified a computational processing pair – non-linear reconstruction (NLR) and raising the image to the power of p enabled the use of many deterministic fields for deconvolution-based 2D imaging applications [26]. However, the imaging results varied with the type of optical field and all of them were generated by highly diffractive masks. The above study leads to an important question. Is it possible to use a refractive lens for deconvolution-based 3D imaging? Lucy-Richardson (LRA) is one of the widely used deconvolution algorithm for deblurring images formed by lens due to depth or motion blur [27, 28]. However, the deconvolution range is limited and so the algorithm cannot be applied to cases with large aberrations. Recently, a deconvolution algorithm, Lucy-Richardson-Rosen algorithm (LRRA) was developed by integrating LRA with NLR and applied to infrared microspectroscopy studies [29]. The performance of the algorithm was significantly better than LRA and NLR. In this study, we have applied LRRA to imaging using a refractive lens to computationally extend the depth of focus of imaging.

Preprints (www.preprints.org) | NOT PEER-REVIEWED | Posted: 1 August 2022 doi:10.20944/preprints202208.0010.v1

The manuscript consists of five sections. The methodology is discussed in the next section. In the third section, the simulation studies are presented. The experimental studies are presented in the fourth section. In the final section, conclusion and future perspectives of the study are discussed.

2. Materials and Methods

The optical configuration of the imaging system is shown in Figure 1. A quasi-monochromatic light source – no spatial coherence and high temporal coherence is considered for illumination. A point object at $\overline{r_o} = (x_o, y_o)$ with an amplitude of $\sqrt{I_o}$ is located at a distance of z_s from a refractive lens with a complex amplitude of $\exp[-j\pi R^2/(\lambda f)]$, where f is the focal length of the lens given as $\frac{1}{f} = \frac{1}{u} + \frac{1}{z_h}$, u is the ideal object distance, z_h is the distance between the refractive lens and the sensor and ideal image distance, λ is the wavelength and R is the radial coordinate given as $R = \sqrt{x^2 + y^2}$. The complex amplitude of light reaching the refractive lens is given as $\psi_1 = C_1\sqrt{I_o}Q\left(\frac{1}{z_s}\right)L\left(\frac{\overline{r_o}}{z_s}\right)$, where $Q(1/z_s) = \exp[j\pi R^2/(\lambda z_s)]$ and $L(\overline{o}/z_s) = \exp[j2\pi(o_x x + o_y y)/(\lambda z_s)]$ are the quadratic and linear phases and C_1 is a complex constant. The complex amplitude after the optical modulator is given as $\psi_2 = C_1\sqrt{I_o}Q\left(\frac{1}{z_1}\right)L\left(\frac{\overline{r_o}}{z_s}\right)$, where $z_1 = \frac{z_s f}{f - z_s}$. The intensity distribution obtained in the sensor plane located at a distance of z_h is the PSF given as

$$I_{PSF} = \left|C_2\sqrt{I_o}L\left(\frac{\overline{r_o}}{z_s}\right)Q\left(\frac{1}{z_1}\right) \otimes Q\left(\frac{1}{z_h}\right)\right|^2, \quad (1)$$

where '⊗' is a 2D convolutional operator. When $z_s = u$, the imaging condition is satisfied, z_1 becomes z_h and a point image is obtained on the sensor. The lateral resolution in the object plane is given as $1.22\lambda z_s/D$, where D is the diameter of the lens. The axial resolution of the system is given as $8\lambda(z_s/D)^2$ and the magnification of the system is given as $M = z_h/z_s$. By the linearity condition of incoherent imaging, the intensity distribution obtained for an object with a function O is given as

$$I_O = |I_{PSF} \otimes O|. \quad (2)$$

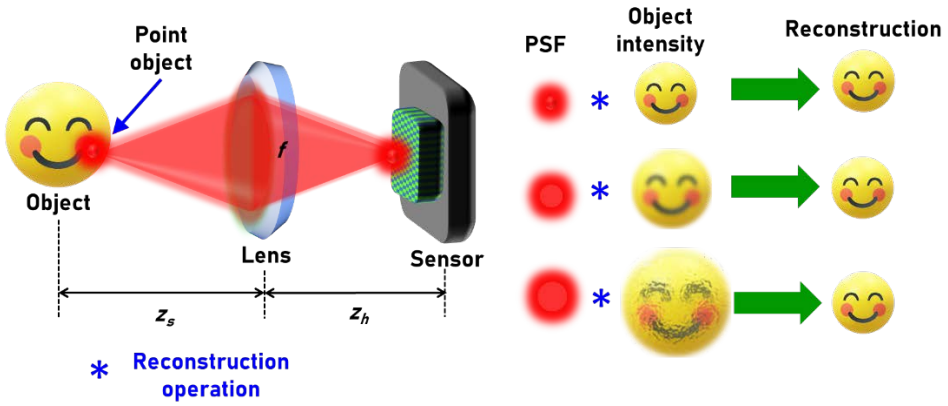

Figure 1. Concept figure of imaging using a refractive lens and computational reconstruction.

In the direct imaging mode, I_O is obtained by sampling of O by I_{PSF} and therefore when the imaging condition is satisfied, the object information gets sampled by the lateral resolution of the system. When the imaging condition is not satisfied, the I_{PSF} is blurred and so is the object information. In indirect imaging mode, the task is to extract O from I_O and I_{PSF}. A direct method to extract O is to cross-correlate I_O and I_{PSF} as $I_R = I_O * I_{PSF}$ which is given as $I_R = I_{PSF} \otimes O * I_{PSF}$. Rearranging the terms, we obtain $I_R = O \otimes I_{PSF} * I_{PSF}$. So, the reconstructed information is the object information sampled by the autocorrelation function of I_{PSF}. The width of the autocorrelation function cannot be smaller than the diffraction limited spot size under normal conditions. When the imaging condition is

Preprints (www.preprints.org) | NOT PEER-REVIEWED | Posted: 1 August 2022 doi:10.20944/preprints202208.0010.v1

satisfied or when a diffuser is used, the autocorrelation function is sharp. When the imaging condition is not satisfied, then the autocorrelation function is blurred making the correlation-based reconstruction not effective. The advanced version of correlation given as a non-linear reconstruction is effective in reducing the background noise arising due to the positive nature of the I_{PSF}s during correlation but is affected by the nature of the intensity distribution [24, 26]. The non-linear reconstruction is given as

$$I_R = \mathcal{F}^{-1}\left\{\left|\tilde{I}_{PSF}\right|^{\alpha}\exp[j\cdot\arg(\tilde{I}_{PSF})]\left|\tilde{I}_O\right|^{\beta}\exp[-j\cdot\arg(\tilde{I}_O)]\right\}, \quad (3)$$

where α and β were varied until a minimum background noise is obtained. While this is one of the robust correlation-based reconstruction methods, LRA uses a different approach involving the calculation of the maximum likelihood solution once again from I_{PSF} and I_O. The $(n+1)^{th}$ reconstructed image in LRA is given as $I_R^{n+1} = I_R^n\left\{\frac{I_O}{I_R^n \otimes I_{PSF}} \otimes I_{PSF}'\right\}$, where I_{PSF}' refers to the complex conjugate of I_{PSF} and the loop is iterated until the maximum likelihood reconstruction is obtained. The initial guess of the LRA is often the recorded image itself and the final solution is a maximum-likelihood solution. As seen in the above equation, there is a forward convolution $I_R^n \otimes I_{PSF}$ and the ratio between this and I_O is correlated with I_{PSF} which is replaced by the NLR which yields a better estimation with reduced background noise and rapid convergence. In this study, the performances of LRA, NLR and LRRA are compared. The schematic of the Lucy-Richardson-Rosen algorithm is shown in Figure 2.

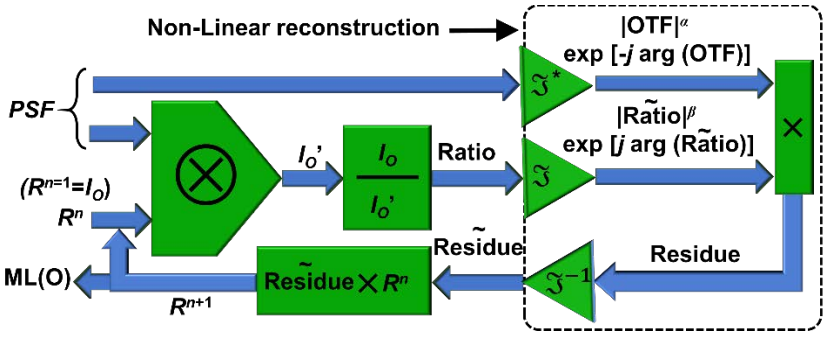

Figure 2. Schematic of LRRA. ML – maximum likelihood; OTF – optical transfer function; n – number of iterations; ⊗ - 2D convolutional operator.

3. Simulation studies

A simulation study was carried out in MATLAB using Fresnel diffraction formulation. A mesh grid was created with a pixel size Δ = 10 μm, λ = 650 nm and 500 × 500 pixels matrix. The values of z_h and f were selected as 0.8 m and 0.4 m respectively and z_s was varied from 0.4 m to 1.2 m in steps of 0.1 m. The recorded PSFs for z_s = 0.4 to 1.2 m in steps of 0.1 m is shown in Figure 3. A test object 'CIPHR' was used and the object intensity distributions were calculated by a convolution between the test object and the PSF. The images of the test object for different cases of axial aberrations are shown in Figure 3. The reconstruction results using LRA, NLR and LRRA are shown in Figure 3. It can be seen that the performance of LRRA is significantly better than LRA and better than NLR. The LRA and NLR had consistent reconstruction conditions such as 20 iterations and α = 0 and β = 0.6. In the case of LRRA, the conditions were changed for every case. The values of (α, β, n) for z_s = 0.4 to 1.2 are (0,0.5,5), (0,0.5,5), (0,0.5,5), (0,0.5,5), (0,0.5,1), (0,0.5,8), (0,0.5,8), (0,0.5,8) and (0, 0.6, 5) respectively. In the case of NLR, the reconstruction improves when the PSF pattern is larger as expected due to improvement in sharpness of autocorrelation function with larger patterns. A 3D simulation was carried out by accumulating the 2D intensity distributions into a cube data. The images of the PSF, object variation from 0.6 to 1 m and the cross-sectional images of reconstructions of NLR, LRA and LRRA are shown

Preprints (www.preprints.org) | NOT PEER-REVIEWED | Posted: 1 August 2022 doi:10.20944/preprints202208.0010.v1

in Figure 5(a)-5(e) respectively. Comparing, 5(c)-5(e), it is seen that NLR and LRRA performed better than LRA, while LRRA exhibited the best performance.

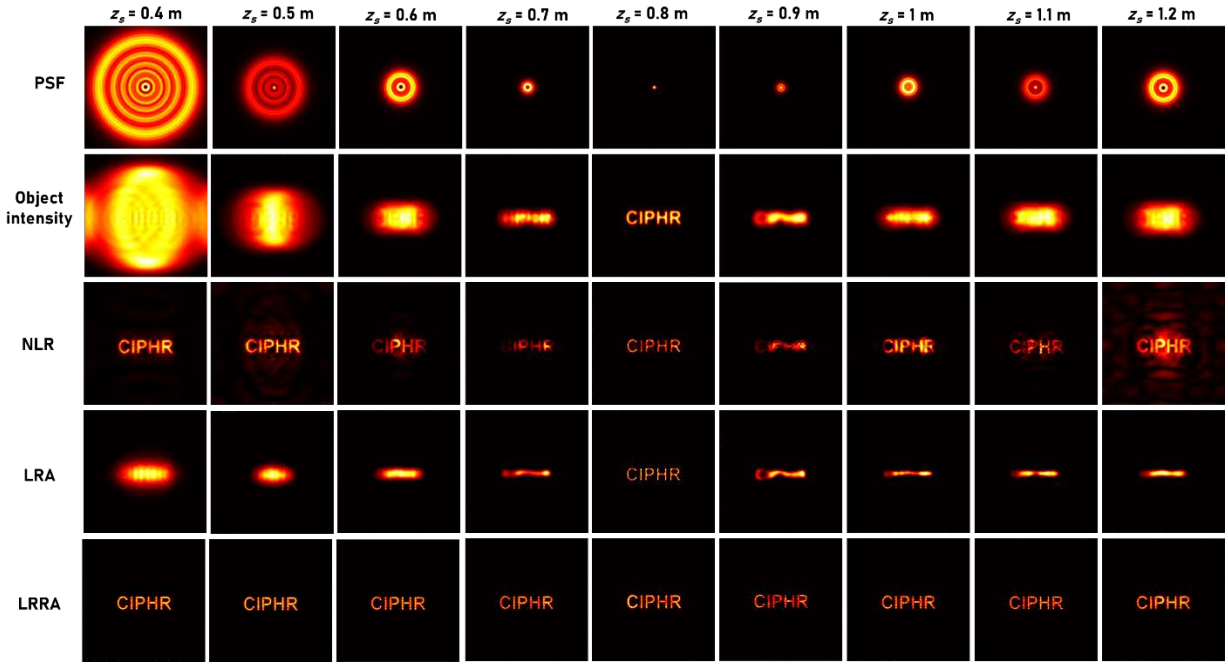

Figure 3 Simulation results of PSF, object intensity and reconstruction results using NLR, LRA and LRRA.

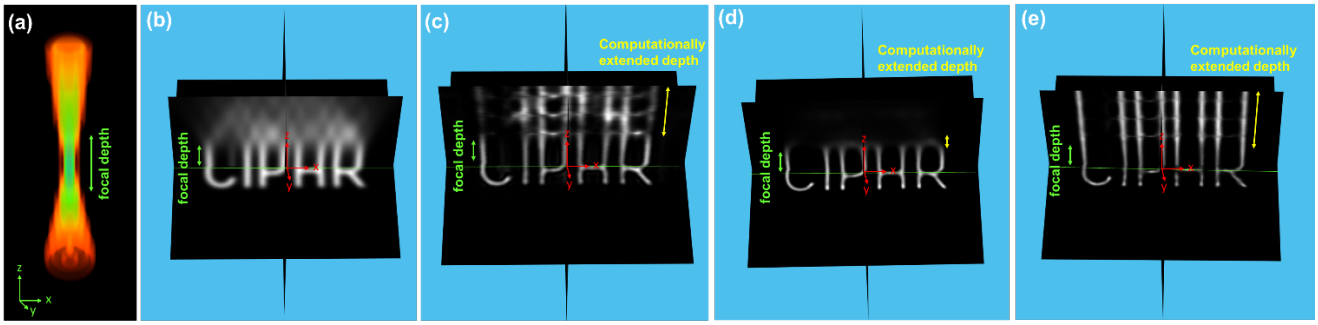

Figure 4 (a) Image of 3D PSF (z_s = 0.6 to 1 m), X-Y cross sectional images obtained from cube data of (b) imaging using a lens, reconstruction using (c) NLR, (d) LRA and (e) LRRA.

4. Experiments

The experimental setup used in this study is shown in Figure 5. This setup consists of a spatially incoherent light source - a high-power LED (Thorlabs, 170 mW, λ = 650 nm and $\Delta\lambda$ = 20 nm). An iris and a refractive lens (L1) of the focal length of 50 mm were used to focus the light from the LED to critically illuminate the object. A pinhole with a diameter of 50 μm was used for recording the PSF library. A refractive lens (L2) with a focal length of f = 35 mm is placed at 2f position between the test object and the image sensor (Quantum QHM495LM 6 Light Webcam) with 480 × 640 pixels and pixel size of ~1.5 μm. The lateral and axial resolutions of the system are 2.2 μm and 40 μm respectively. A neutral-density filter (ND 1.5) was placed between the image sensor and the L2 to reduce the light intensity. In the first step, the PSF library was recorded by shifting the location of the pinhole along the +z and -z directions in steps of 0.25 mm. Then, the pinhole was replaced by the test object, and the corresponding images were recorded in identical planes to that of the PSF. The PSF library and the object intensity distributions were then fed into the reconstruction algorithm and the images were deconvolved. The experimental set up is highly economical and can be constructed with as low as < 20 €. Three test objects were considered for imaging experiments. The first test object is a double slit like object with a

Preprints (www.preprints.org) | NOT PEER-REVIEWED | Posted: 1 August 2022 doi:10.20944/preprints202208.0010.v1

size 1.5 × 0.28 mm (L × B). The images of the PSFs recorded at z_s = 7 cm, 7.1 cm and 7. 2 cm, the corresponding direct imaging (DI) results of object and reconstruction results using LRA (n = 20), NLR (α = 0.2, β = 0.7) and LRRA (α = 0.6, β = 0.9) with n = 2, 12 and 12 for the above three cases are shown in Figure 6. The second test object is a cross like object with a size 3.06 × 3.4 mm (L × B).The images of the PSFs recorded at z_s = 7 cm, 7.2 cm and 7. 4 cm, the corresponding direct imaging (DI) results of object and reconstruction results using LRA (n = 20), NLR (α = 0.2, β = 0.7) and LRRA (α = 0.8, β = 0.9, n = 10), (α = 0.8, β = 1, n = 10) and (α = 0.8, β = 0.9, n = 15) for the above three cases are shown in Figure 7. The third test object consist of two circular objects each with a radius of 360 μm. The images of the PSFs recorded at z_s = 7 cm, 7.2 cm and 7. 4 cm, the corresponding direct imaging (DI) results of object and reconstruction results using LRA (n = 20), NLR (α = 0.2, β = 0.7) and LRRA (α = 0.6, β = 0.9, n = 12), (α = 0.8, β = 1, n = 15) and (α = 0.8, β = 1, n = 15) for the above three cases are shown in Figure 8.

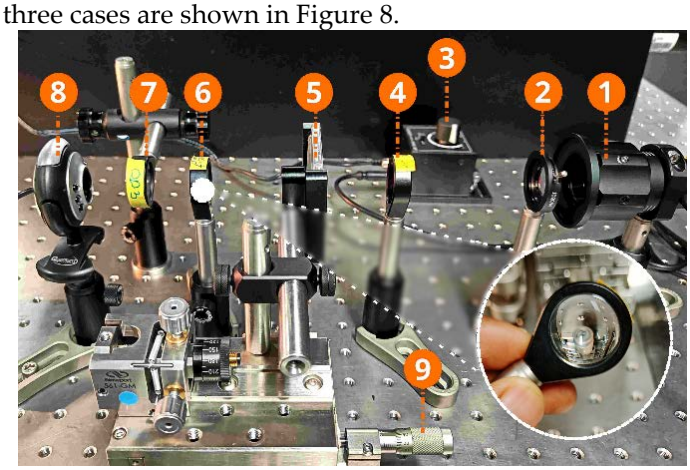

Figure 5. Photograph of the experimental setup: (1) LED source, (2) Iris, (3) LED power source, (4) Lens L1 (f = 50 mm), (5) Test object, (6) Lens L2 (f = 35 mm), (7) ND filter (ND 1.5), (8) Image sensor and (9) XY stage movement controller.

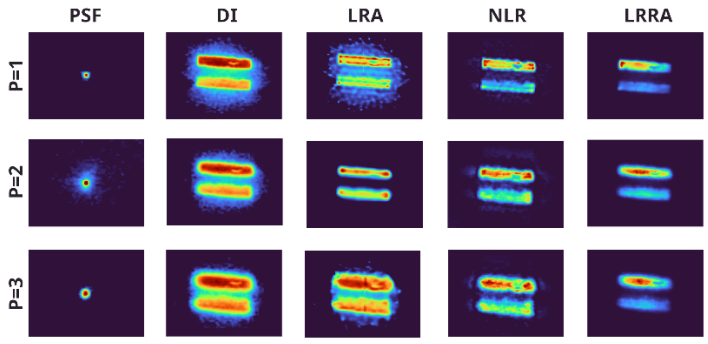

Figure 6. Images of the PSF, DI of the test object – 1, reconstruction results using LRA, NLR and LRRA.

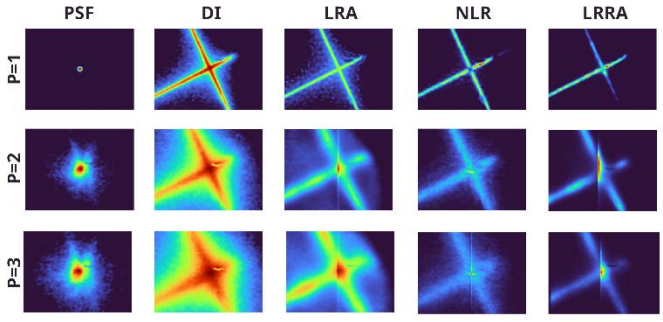

Figure 7. Images of the PSF, DI of the test object – 2, reconstruction results using LRA, NLR and LRRA

Preprints (www.preprints.org) | NOT PEER-REVIEWED | Posted: 1 August 2022 doi:10.20944/preprints202208.0010.v1

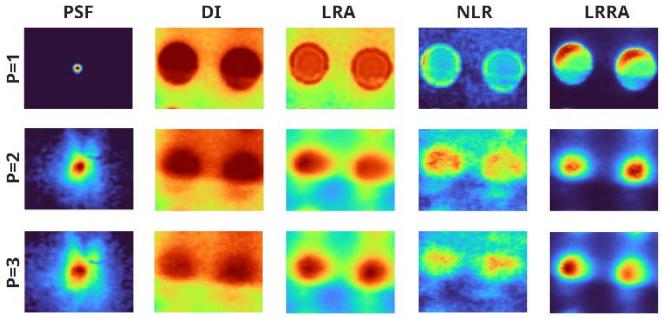

Figure 8. Images of the PSF, DI of the test object – 3, reconstruction results using LRA, NLR and LRRA.

The structural similarity index (SSIM) of the reconstructed images was calculated with respect to the reference image recorded without aberration for direct imaging, LRA, NLR, and LRRA. The maps of the SSIM for the above cases are shown in Fig. 9. It should be noted that the presence of stray light in the recorded images could significantly affect the SSIM index. This could be attributed to the slight variations observed in Fig. 9. The SSIM values are plotted as shown in Fig. 10. It can be seen that LRRA performed better than both LRA and NLR techniques.

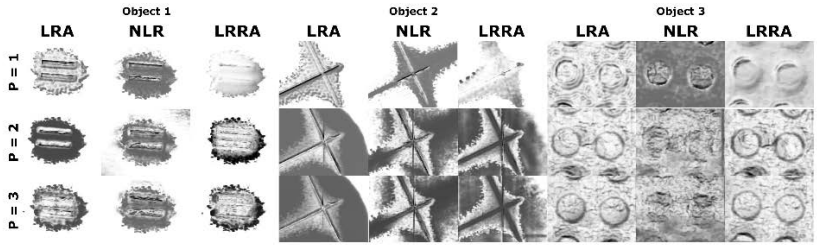

Figure 9. SSIM maps for the test objects with respect to the direct imaging and the reconstruction results using LRA, NLR and LRRA.

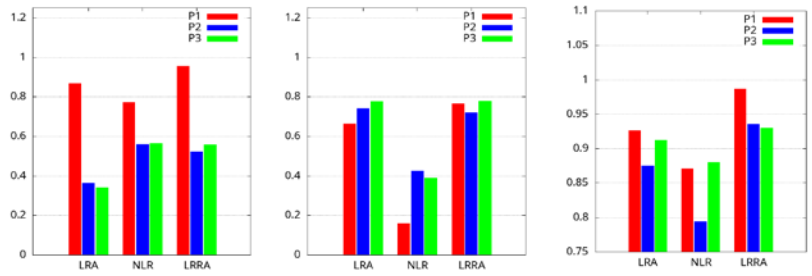

Figure 10. SSIM values of the test objects with respect to the direct imaging and the reconstruction results.

5. Conclusions

A refractive lens is one of the simplest optical elements that can be used for 2D imaging with spatially incoherent light. However, the depth of focus of imaging is limited to ~λ/NA^2 beyond which the object information becomes blurred. There are many computational techniques that can be used to deblur the object information but are often limited to a smaller range of axial aberrations [30-32]. In this study, a recently developed computational technique called the LRRA has been implemented for deep deconvolution of images formed by a refractive lens and compared against NLR and LRA. The performance of LRRA seems significantly better than LRA and better than NLR in both simulation as well as experimental studies. Since the simulation and experimental studies confirm the possibility of a higher range of deconvolution, we believe that this study will benefit 3D imaging using spatially incoherent light. In this study, a nearly 3D imaging has been demonstrated.

Author Contributions: Conceptualization, V. A.; methodology, experiments, P. A. .;P and A. S. J. F. R.; V. A.; software, V. A; P.A.P.; validation, P. A. P.; A. S. J. F. R.; T. K.; and V. A.; formal analysis, T. K.; S. H. N.; D. S.; P. A. P.; F. G. A.; S. G.; S-M. V.; A. B.; A. N. K. R.; T. K.; investigation, V. A.; S. J.; A. T.; K. K.; S. P. R.; R. G.; resources, V. A.; A. T.; K. K.; S. J.; S. P.; R. G.; data curation, P. A. P.; A. S. J. F. R.; V. A.; writing—original draft preparation, P. A. P.; A. S. J. F. R.; V. A.; writing—review and editing, All the authors.; visualization, A. S. J. F. R.; P. A. P.; V. A.; supervision, V. A.; S. J.; R. G.; A. T.; S. P.; K. K.; project administration, V. A.; S. J.; A. T.; K. K.; S. P.; R. G.; funding acquisition, V. A., S. J.; A. T.; S. P.; K. K.; R. G.; All authors have read and agreed to the published version of the manuscript.

Funding: D. S.; S. H. N.; T. K.; S. J. are grateful for the financial support via ARC Linkage LP190100505 project. P. A. P.; V. A.; A. S. J. F. R.; S- M. V. acknowledges the European Union's Horizon 2020 research and innovation programme grant agreement No. 857627 (CIPHR). T. K., K. K., and A. T. acknowledge support from European Regional Development Fund project "Emerging orders in quantum and nanomaterials" (TK134). A. N. K. R. acknowledges the support from the State Education Development Agency (SEDA), Republic of Latvia (Project Number: 1.1.1.2/VIAA/3/19/436) and European Regional Development Fund (1.1.1.5/19/A/003).

Data Availability Statement: The experimental data corresponding to this study are given within the manuscript. Theoretical simulation data are openly available in zenodo.org. DOI: 10.5281/zenodo.6928454.

Acknowledgments: P. A. P.; S-M. V.; A. S. J. F. R.; V. A thank Tiia Lillemaa for the administrative support.

Conflicts of Interest: The authors declare no conflict of interest.

References

1. Rosen, J.; Vijayakumar, A.; Kumar, M.; Rai, M. R.; Kelner, R.; Kashter, Y.; Bulbul, A.; and Mukherjee, S. Recent advances in self-interference incoherent digital holography. *Adv. Opt. Photon*. **2019**, *11*, 1-66.
2. Lichtman, J.W.; and Conchello, J.A. Fluorescence microscopy. *Nat. methods* **2005**, *2*, 910-919.
3. Kim, M.K. Adaptive optics by incoherent digital holography. *Opt. Lett*. **2012**, *37*, 2694-2696.
4. Liu, J.P.; Tahara, T.; Hayasaki, Y.; and Poon, T.-C. Incoherent digital holography: a review. *Appl. Sci.* **2018**, *8*, 143.
5. Poon, T.-C. Optical scanning holography-a review of recent progress. *J. Opt. Soc. Korea* **2009**, *13*, 406-415.
6. Rosen, J.; Alford, S.; Anand, V.; Art, J.; Bouchal, P.; Bouchal, Z.; Erdenebat, M.U.; Huang, L.; Ishii, A.; Juodkazis, S.; et al. Roadmap on recent progress in FINCH technology. *J. Imaging* **2021**, *7*, 197.
7. Murty, M. V. R. K.; and Hagerott, E. C. Rotational shearing interferometry. *Appl. Opt*. **1966**, *5*, 615.
8. Sirat, G.; and Psaltis, D. Conoscopic holography. *Opt. Lett*. **1985**, *10*, 4.
9. Rosen, J.; and Brooker, G. Digital spatially incoherent Fresnel holography. *Opt. Lett.* **2007**, *32*, 912-914.
10. Kim, M. K. Incoherent digital holographic adaptive optics. *Appl. Opt*. **2013**, *52*, A117.
11. Kelner, R.; Rosen, J.; and Brooker, G. Enhanced resolution in Fourier incoherent single channel holography (FISCH) with reduced optical path difference. *Opt. Express* **2013**, *21*, 20131-20144.
12. Vijayakumar, A.; Kashter, Y.; Kelner, R.; and Rosen, J. Coded aperture correlation holography–a new type of incoherent digital holograms. *Opt. Express* **2016**, *24*, 12430-12441.
13. Ables, J.G. Fourier transform photography: a new method for X-ray astronomy. *Publ. Astron. Soc. Aust.* **1968,** *1*, 172-173.
14. Dicke, R.H. Scatter-hole cameras for x-rays and gamma rays. *Astrophys. J*. **1968**, *153*, L101.
15. Cieślak, M.J.; Gamage, K.A.; and Glover, R. Coded-aperture imaging systems: Past, present and future development–A review. *Radiat. Meas.* **2016**, *92*, 59-71.
16. Anand, V.; Rosen, J.; and Juodkazis, S. Review of engineering techniques in chaotic coded aperture imagers. *Light: Advanced Manufacturing* **2022**, *3*, 24.
17. Vijayakumar, A.; and Rosen, J. Interferenceless coded aperture correlation holography–a new technique for recording incoherent digital holograms without two-wave interference. *Opt. Express* **2017**, *25*, 13883-13896.
18. Singh, A.K.; Pedrini, G.; Takeda, M.; and Osten, W. Scatter-plate microscope for lensless microscopy with diffraction limited resolution. *Sci. Rep.* **2017**, *7*, 10687.
19. Antipa, N.; Kuo, G.; Heckel, R.; Mildenhall, B.; Bostan, E.; Ng, R.; Waller, L. DiffuserCam: Lensless single-exposure 3D imaging. *Optica* **2018**, *5*, 1–9.
20. Sahoo, S. K.; Tang, D.; and Dang, C. Single-shot multispectral imaging with a monochromatic camera. *Optica* **2017**, *4*, 1209-1213.
21. Vijayakumar, A.; and Rosen, J. Spectrum and space resolved 4D imaging by coded aperture correlation holography (COACH) with diffractive objective lens. *Opt. Lett*. **2017**, *42*, 947.

22. Anand, V.; Ng, S.H.; Maksimovic, J.; Linklater, D.; Katkus, T.; Ivanova, E.P.; and Juodkazis, S. Single shot multispectral multidimensional imaging using chaotic waves. *Sci. Rep*. **2020**, *10*, 1-13.
23. Anand, V.; Ng, S.H.; Katkus, T.; and Juodkazis, S. Spatio-spectral-temporal imaging of fast transient phenomena using a random array of pinholes. *Adv. Photonics Res.* **2021**, *2*, 2000032.
24. Rai, M.R.; Vijayakumar, A.; and Rosen, J. Non-linear adaptive three-dimensional imaging with interferenceless coded aperture correlation holography (I-COACH). *Opt. Express*. **2018**, *26*, 18143-18154.
25. Horner, J. L.; and Gianino, P. D. Phase-only matched filtering. *Appl. Opt*. **1984**, *23*, 812.
26. Smith, D.; Gopinath, S.; Arockiaraj, F.G.; Reddy, A.N.K.; Balasubramani, V.; Kumar, R.; Dubey, N.; Ng, S.H.; Katkus, T.; Selva, S.J.; Renganathan, D.; Kamalam, M.B.R.; John Francis Rajeswary, A.S.; Navaneethakrishnan, S.; Inbanathan, S.R.; Valdma, S.-M.; Praveen, P.A.; Amudhavel, J.; Kumar, M.; Ganeev, R.A.; Magistretti, P.J.; Depeursinge, C.; Juodkazis, S.; Rosen, J.; Anand, V. Nonlinear Reconstruction of Images from Patterns Generated by Deterministic or Random Optical Masks—Concepts and Review of Research. *J. Imaging* **2022**, *8*, 174.
27. Richardson, W. H. Bayesian-Based Iterative Method of Image Restoration. *J. Opt. Soc. Am*. **1972**, *62*, 55.
28. Lucy, L. B. An iterative technique for the rectification of observed distributions. *Astron. J.* **1974**, *79*, 745.
29. Anand, V.; Han, M.; Maksimovic, J.; Ng, S. H.; Katkus, T.; Klein, A. R.; Bambery, K. R.; Tobin, M. J.; Vongsvivut, J.; Juodkazis, S. Single-shot mid-infrared incoherent holography using Lucy Richardson Rosen algorithm. *Opto-Electron. Sci.* **2022**, *1*, 210006.
30. Beck, A.; and Teboulle, M. Fast gradient-based algorithms for constrained total variation image denoising and deblurring problems. *IEEE Trans. Image Process*. **2009**, *18*, 2419.
31. Biemond, J.; Lagendijk, R.L.; and Merserau, R.M. Iterative methods for image deblurring. *Proc. IEEE* **1990**, *78*, 856.
32. Wang R.; Tao D. Recent progress in image deblurring. arXiv preprint arXiv:1409.6838. **2014** Sep 24.